The Radiation Transport Model for Physical Cryptographic Verification of Nuclear Warheads

Jayson R. Vavrek, Brian S. Henderson, Areg Danagoulian

Laboratory for Nuclear Security and Policy, Massachusetts Institute of Technology, Cambridge, MA, USA, jvavrek@mit.edu, bhender1@mit.edu, aregjan@mit.edu

INTRODUCTION

Nuclear resonance fluorescence (NRF)—the resonant absorption and subsequent re-emission of a photon by a nucleus—is a powerful isotope-specific measurement technique. NRF has become popular in recent years in a wide range of applications, including physical cryptographic verification of nuclear warheads [1, 2], measurements of spent fuel [3], cargo security [4, 5], and investigations of fundamental nuclear structure [6]. Accurate NRF radiation transport models—both mathematical models and simulation codes—are therefore critical for evaluating the utility of NRF measurements in these settings or in new applications. In particular, an accurate semi-analytical model of expected NRF rates offers a much more efficient means of iteratively designing NRF experiments than full Monte Carlo simulation.

To this end, this paper focuses on recent verification and validation work on the semi-analytical fixed-source NRF photon transport model that arises in measurements such as the physical cryptographic verification of nuclear warheads. We first present an outline of the high-precision semi-analytical model used to predict NRF count rates in simulated and experimental geometries. We then show updated results of verification simulations using the G4NRF Monte Carlo code, present preliminary results of validation experiments, and conclude with a discussion of future work.

THEORY

In a nuclear resonance fluorescence interaction, a nucleus resonantly absorbs a photon of energy E approximately equal to a nuclear resonance energy E_r and transitions to an excited state [7]. The intrinsic widths of these interactions are $\Gamma_r \sim 1$–100 meV, but are increased by Doppler broadening to $\Delta \sim 1$ eV. The cross section for an NRF interaction is therefore most accurately given by a Doppler-broadened Breit-Wigner distribution:

$$\sigma_{\mathrm{NRF}}(E) = 2\pi^{1/2} g_r \left(\frac{\hbar c}{E_r}\right)^2 \frac{b_{0,r}}{\sqrt{t}} \int_{-\infty}^{\infty} \exp\left[-\frac{(x-y)^2}{4t}\right] \frac{dy}{1+y^2}, \tag{1}$$

where

$$x \equiv 2(E - E_r)/\Gamma_r, \tag{2}$$

$$t \equiv (\Delta/\Gamma_r)^2, \tag{3}$$

$$g_r \equiv \frac{2J_r + 1}{2(2J_0 + 1)}, \tag{4}$$

where J_0 and J_r are the spins of the ground state and resonant level at E_r, respectively, and $b_{0,r}$ is the branching ratio between the two states. On timescales O(fs), the excited nucleus transitions back to its ground state, releasing a photon ("fluorescing") with energy E' determined by the nuclear level structure of the isotope and branching ratios of the particular level. NRF therefore provides a signature of the measurement object that is specific to its isotopic composition.

A simplified 1D, single-isotope schematic of a transmission NRF measurement is shown in Fig. 1. In this configuration, a quasi-parallel initial photon spectrum $\phi_0(E)$ (typically ~2 MeV bremsstrahlung) is incident on the measurement object of thickness D. In a warhead verification scenario, the measurement object is the candidate nuclear warhead to be verified. The flux transmitted through the measurement object encodes the value of D through

$$\phi_t(E) = \phi_0(E) \exp(-D[\mu_{\mathrm{NRF}}(E) + \mu_{\mathrm{nr}}(E)]), \tag{5}$$

where $\mu = N\sigma$ in general for a number density N and the "nr" subscript denotes attenuation via non-resonant processes (Compton scattering, photoelectric absorption, etc.). The transmitted flux then goes on to interact with the "reference foil" of thickness X, which must be constructed of the same isotope that is to be analyzed in the measurement object.[1] The predicted double-differential rate of NRF detections by an HPGe detector at angle θ to the beamline is then determined by the rate of NRF photon generation in the reference foil but reduced by the measurement object thickness D through Eq. (5):

$$\frac{\mathrm{d}^2 n}{\mathrm{d}E\,\mathrm{d}\Omega} = \phi_t(E)\, b\, \mu_{\mathrm{NRF}}(E) \frac{W(\theta)}{4\pi} \times \frac{1 - \exp\left[-X\mu_{\mathrm{eff}}(E, E', \theta)\right]}{\mu_{\mathrm{eff}}(E, E', \theta)} \epsilon_{\mathrm{int}}(E') P_f(E'). \tag{6}$$

Here

$$\mu_{\mathrm{eff}}(E, E', \theta) \equiv \mu_{\mathrm{NRF}}(E) + \mu_{\mathrm{nr}}(E) + \frac{\mu_{\mathrm{nr}}(E')}{\cos\theta} \tag{7}$$

is the "effective" attenuation in the foil, b is the branching ratio for the transition of energy E', $W(\theta)$ is the angular anisotropy, $\epsilon_{\mathrm{int}}(E')$ is the intrinsic full-peak efficiency of the detector, and $P_f(E')$ is the probability of photon transmission through detector shielding. Integration of Eq. (6) over all E and the Ω of the detector then gives the rate of NRF photon detections. Due to the intrinsic resolution of the detector, the NRF emission line appears as a Gaussian peak with standard deviation O(1 keV) rather than the lineshape given in Eq. (1).

[1] In a traditional NRF measurement as described here, the reference foil thickness X is known, so that the only unknown variable is D. In a physical cryptographic verification measurement, the value of X must be kept secret from the independent verifier to prevent reconstruction of the warhead D. A relative ("template") measurement scheme is therefore used, whereby X is kept secret but constant between NRF measurements of a candidate warhead to be verified and a previously-authenticated warhead.

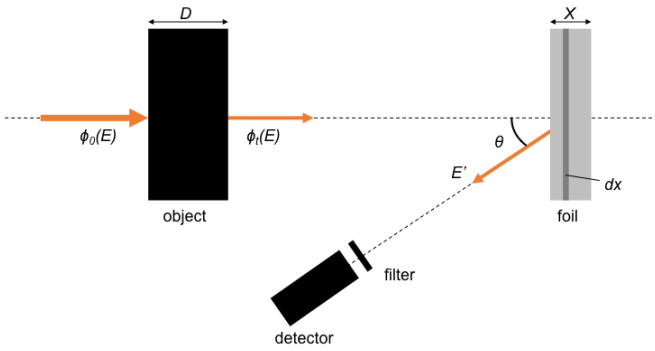

Fig. 1. Single-isotope, 1D schematic of a transmission NRF measurement of the thickness D of the measurement object. A narrow beam of the interrogating flux $\phi_0(E)$ impinges on the measurement object, and the flux $\phi_t(E)$ transmitted through the object impinges on a reference foil (of thickness X) composed of the same isotope as the target. The rate of NRF photons generated in the foil and subsequently observed by the detector is reduced from the foil-only case by the presence of the measurement object, allowing the object's thickness to be estimated.

METHODS

Verification: Monte Carlo simulation

In order to verify the semi-analytical model of Eq. (6), verification simulations are carried out using the G4NRF [8] Monte Carlo code package for Geant4 [9]. Simulation geometries consist of simplified setups akin to Fig. 1 (as opposed to more realistic experimental setups) in order to compare the predictions of Eq. (6) to simulation in a straightforward manner. The measurement object and foil are both square plates constructed from a single isotope: U-238 or Al-27. The incident flux $\phi_0(E)$ is a parallel pencil beam with magnitude zero everywhere except for a uniform distribution of energies within narrow brackets (±25 eV) around the NRF resonances of interest (2.176, 2.209, and 2.245 MeV for U-238, and 2.212 MeV for Al-27). The energies of all photons leaving the foil in the cone defined by $\theta \leq \pi/4$ are recorded, and the numbers of photons in the 1 keV-wide resonant energy bins are extracted for comparison against Eq. (6).

A more complicated verification test is carried out by retrodicting the counts in the simulated geometries of Ref. [1]. An expanded version of Eq. (6) that accounts for multi-layer objects and foils is used to predict the number of NRF counts for two U-238 lines (2.176, 2.209 MeV) and one Pu-240 line (2.443 MeV) under a more realistic simulated bremsstrahlung photon beam.

In this case, the model calculations are straightforward: $\epsilon_{\text{int}}(E')$ and $P_f(E')$ are both 1, since no detector response is simulated; $\mu_{\text{eff}}(E, E', \theta)$ is computed using Eq. (1) (resonant) and NIST XCOM tables (non-resonant); $W(\theta)$ is known [10]; b is approximately known [11, e.g.]; and $\phi_0(E)$ is determined by the number of primaries (or the simulated bremsstrahlung distribution). The integral over Ω between 0 and $\pi/4$ is straightforward to implement numerically, and the integral over E is computed between $E \pm 4\Delta$ for numerical stability. Finally, the foil thickness X and object thickness D are left as variable parameters.

Validation: experimentation

Validation experiments were performed using the Van de Graaff electrostatic accelerator at MIT's High Voltage Research Laboratory. A 2.52 MeV, 25 μA electron beam was directed at a Cu+Au bremsstrahlung radiator, producing a 2.52 MeV endpoint interrogation flux $\phi_0(E)$. Various measurement objects were constructed from DU, Pb, and plastic plates as part of a series of proof-of-concept warhead verification experiments [2]. The foil comprised DU plates of total thickness 0.32 cm followed by 6.35 cm of Al plates. NRF spectra emitted from the foil were measured using three Ortec HPGe detectors and recorded using Lynx Digital Signal Analyzers. Observed NRF rates were computed by fitting the NRF spectra with a sum of Gaussian peaks and an exponential background; the NRF rates under the peaks (above the continuum) were then normalized by the beam current and live time of the acquisition period.

The expected count rates in the experiments were computed using the aforementioned expanded version of Eq. (6). The incident flux $\phi_0(E)$ was computed in a standalone Geant4 simulation of the electron beam interaction with a detailed radiator geometry. The intrinsic efficiency $\epsilon_{\text{int}}(E') \sim 0.14$ was similarly computed using a standalone simulation of photon flight from the DU foil to the detector, and a similar geantino flight simulation was used to determine the geometric efficiency $\epsilon_{\text{geom}} \sim 1.3 \times 10^{-3}$. The NRF and non-resonant cross sections were computed as above, and the $P_f(E')$ was similarly calculated using NIST XCOM tables and 2.54 cm of Pb.

RESULTS

An example of a direct comparison of NRF count rates between the semi-analytical model of Eq. (6) and the Geant4+G4NRF simulation for the geometry described in Ref. [1] is shown in Fig. 2. Across all completed verification calculations, the semi-analytical model agrees with the Geant4+G4NRF simulations to within ~5%.

An example NRF spectrum from the experimental campaign in Ref. [2] is shown in Fig. 3. In this particular spectrum, the ratios of predicted-to-observed count rates (using Eq. (6)) in the U-238 NRF peaks at 2.176 MeV and 2.245 MeV are 1.11 ± 0.12 and 1.11 ± 0.16, respectively, while the ratio for the Al-27 peak at 2.212 MeV is 0.93 ± 0.06. Across all different validation scenarios, the semi-analytical model appears to be consistent with observed data; however, preliminary comparisons of Eq. (6) vs Geant4+G4NRF simulations of the full experimental geometry indicate that Eq. (6) may be underpredicting the NRF rates by a factor of ~1.3, leading to artificially good agreement between Eq. (6) and the data. Such a dis-

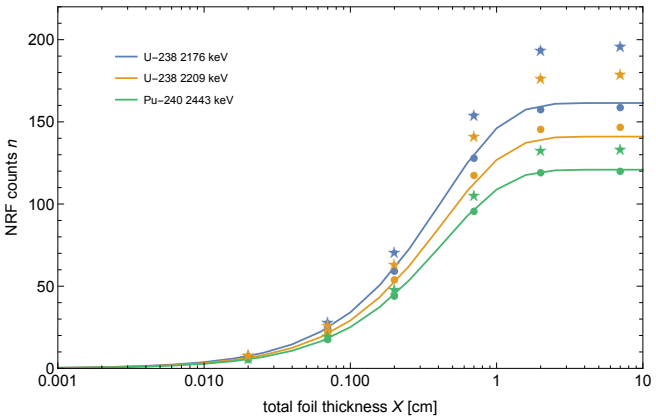

Fig. 2. Verification of Eq. (6) (solid curves) against G4NRF (circles and stars) for two resonances of U-238 and one of Pu-240 with the "Black Sea" measurement object in Ref. [1] for various foil thicknesses X. Eq. (6) does not account for the "notch refill" effect, whereby high-E photons are small-angle scattered down to the NRF resonance energy; stars denote the raw simulation results (including notch refill) while circles denote the refill-subtracted results.

crepancy may arise from various approximations built into the semi-analytical model to keep Eq. (6) tractable, such as the use of an average θ in Eq. (7) despite the use of the more accurate geantino flight estimate of $\epsilon_{\text{geom}} = \Omega/4\pi$. This effect will be explored in future work.

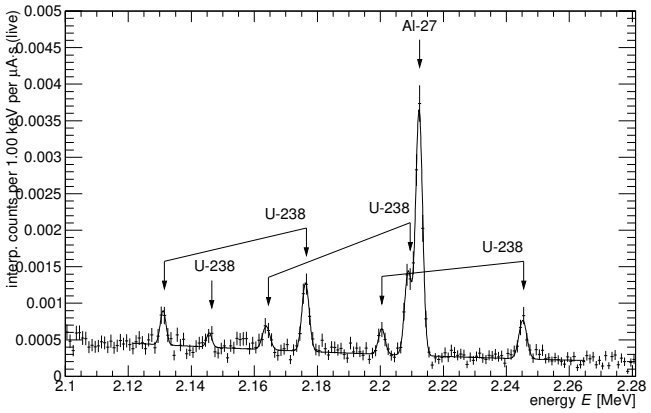

Fig. 3. NRF spectrum and fit resulting from a DU+Al foil and DU+plastic measurement object, from Ref. [2].

CONCLUSIONS

We have performed verification and validation tests of the semi-analytical radiation transport model (Eq. (6)) arising in physical cryptographic NRF measurements. In general, the theory vs simulation verification tests are consistent to within 5%, indicating that the semi-analytical model agrees well with Geant4+G4NRF Monte Carlo results. The semi-analytical model is consistent with experimental data, but may be artificially so, based on preliminary Geant4+G4NRF simulations of the complete experiment. The direct comparison of Geant4+G4NRF to experimental results will therefore be discussed in a more comprehensive forthcoming paper, as will an analysis of systematics and possible relative (rather than absolute) measurements. Other future work will focus on building radiation transport models of the continuum background underneath the NRF peaks, as the continuum itself may encode useful information in certain measurement contexts.

ACKNOWLEDGMENTS

This work was funded in-part by the Consortium for Verification Technology under Department of Energy National Nuclear Security Administration award number DE-NA0002534. BSH gratefully acknowledges the support of the Stanton Foundation's Nuclear Security Fellowship program.

REFERENCES

1. R. S. KEMP, A. DANAGOULIAN, R. R. MACDONALD, and J. R. VAVREK, "Physical cryptographic verification of nuclear warheads," *Proceedings of the National Academy of Sciences*, **113**, *31*, 8618–8623 (2016).
2. J. R. VAVREK, B. S. HENDERSON, and A. DANAGOULIAN, "Experimental demonstration of an isotope-sensitive warhead verification technique using nuclear resonance fluorescence," *arXiv preprint arXiv:1712.02904* (2017).
3. B. J. QUITER, B. A. LUDEWIGT, V. V. MOZIN, C. WILSON, and S. KORBLY, "Transmission nuclear resonance fluorescence measurements of ^{238}U in thick targets," *Nuclear Instruments and Methods in Physics Research Section B: Beam Interactions with Materials and Atoms*, **269**, *10*, 1130–1139 (2011).
4. W. BERTOZZI and R. J. LEDOUX, "Nuclear resonance fluorescence imaging in non-intrusive cargo inspection," *Nuclear Instruments and Methods in Physics Research Section B: Beam Interactions with Materials and Atoms*, **241**, *1*, 820–825 (2005).
5. J. PRUET, D. MCNABB, C. HAGMANN, F. HARTEMANN, and C. BARTY, "Detecting clandestine material with nuclear resonance fluorescence," *Journal of Applied Physics*, **99**, *12*, 123102 (2006).
6. U. KNEISSL, H. PITZ, and A. ZILGES, "Investigation of nuclear structure by resonance fluorescence scattering," *Progress in Particle and Nuclear Physics*, **37**, 349 – 433 (1996).
7. F. R. METZGER, "Resonance fluorescence in nuclei," *Prog. in Nuc. Phys*, **7**, 54 (1959).
8. D. V. JORDAN and G. A. WARREN, "Simulation of nuclear resonance fluorescence in Geant4," in "Nuclear Science Symposium Conference Record, 2007. NSS'07. IEEE," IEEE (2007), vol. 2, pp. 1185–1190.
9. S. AGOSTINELLI, J. ALLISON, K. AMAKO, J. APOSTOLAKIS, H. ARAUJO, P. ARCE, M. ASAI, D. AXEN, S. BANERJEE, G. BARRAND, ET AL., "GEANT4—a simulation toolkit," *Nuclear Instruments and Methods in Physics Research Section A: Accelerators, Spectrometers,*

Detectors and Associated Equipment, **506**, *3*, 250–303 (2003).
10. D. R. HAMILTON, "On Directional Correlation of Successive Quanta," *Phys. Rev.*, **58**, 122–131 (Jul 1940).
11. E. BROWNE and J. TULI, *Nuclear Data Sheets*, **127** (2015).